Robust Hierarchical Control Design and Implementation for the Hybrid Shipboard Microgrid

Farooq Alam, Arsalan Rehmat, Syed Sajjad Zaidi, Maria Ashraf, Asif Gulraiz, Bilal M. Khan
(farooq.phdee19pnec, arsalan.msee19pnec)@student.nust.edu.pk
Department of Electronics and Power Engineering,
National University of Sciences and Technology, Islamabad, Pakistan

***Abstract*—Shipboard microgrid power regulation, optimization, integration, and control are getting more attention. Renewable energy source integrations have become common in shipping ports and on short-distance cruises and ferries. This is due to high carbon emissions from old transportation systems and the continuous usage of fossil fuels for ships. The variations in circulating power that are exchanged between inverters during load shifts can be affected by different line impedances and impact the instantaneous power, especially when unmeasured disturbances occur due to AC/DC load changes on the ship. We extended our work with practical validation of control schemes on the NVIDIA Jetson Nano System hardware setup. In this paper, we have presented the analytical notion of our proposed hierarchical controller robustness for hybrid shipboard Microgrid systems. The multiple distributed generators and renewable energy resource integrations are considered. The load variations of classical PI and sliding mode control-based control design are computed under a variety of grid conditions, and load variations are presented for both AC and DC loads. The system stability and control law formulation is carried out and verified by simulation as well as practical implementations. Simulations and hardware tests of the secondary controller are established from MATLAB/SIMULINK. From the practical results, we show that the proposed secondary control architecture is a more robust hierarchical control structure for the hybrid shipboard microgrid system.**

***Index Terms*—Hardware Implementations; Renewable Energy Resources; Robust Secondary Control Scheme; Sliding Mode Control; Shipboard Microgrid System.**

I. Introduction

Nowadays, due to the widespread penetration of alternating current (AC) and direct current (DC) renewable systems, increasing research efforts are dedicated to the development of hybrid shipboard Microgrid (SMG). As both AC and DC type loads can operate together, hybrid SMG is able to be shared for power for their more efficient operations [1]. In light of the microgrid concept as a radical change of the traditional power system, many mathematical models and analysis techniques need to be examined and enhanced for the controlling of hybrid SMG.

Microgrids can produce power from photo-voltaic (PV) module. The power supplied by these sources is linked to power grids by power electronics inverters. These inverters ensure power equilibrium in a three-phase system, voltage set point tracking, and residual load transfer in the main grid [2]. Several strategies have been projected to solve the above issues and have been integrated into a hierarchical control architecture in order to three levels in this hierarchy. Short-range ships and seaports should consider substituting energy sources and energy storage technologies [3].

An additional strategy to reduce carbon emissions in shipping ports is to use electricity from shore power during "cold ironing", which is a process that connects ships to the power network. Among other things, cold ironing lowers ship's emissions when they are at the dock boosting the electricity demand in the power network. However, technology development for the electrification of port facilities and other electrical expenses for presenting electricity to seaports is designed far away from the network [4].

We present an SMG solution enabling mobile cold-ironing capabilities offering local energy production from RES on ships and enabling electricity exchange with other ships in the port. This concept can be achieved through either public-private partnerships or shipowners investing in providing battery-powered yachts or ferries [5]. Moreover, Europe's seaport growth aims to reduce the transport industry emissions from the seaport sector and create a sustainable future for ports and shipowners.

By combining AC and DC power grids, a microgrid can distribute power. Stable voltage and frequency are the primary functions of the microgrid's control design. In conventional power systems, the current-controller-based proportional control designs were used to operate locally for every distributed IC, even though centralized control architectures are typically employed for primary controllers [6]. This decentralized droop controller provides smooth power flow and stability to the system. However, voltages and frequency variations due to grid transitions or dynamic load variations can cause system abnormalities. Therefore, a robust control strategy is required to overcome this issue.

Academicians and researchers worldwide are discussing more advanced control strategies to address the widespread employment of renewable energy resources (RES). Additionally, conventional controller techniques are less capable of addressing the complexities and uncertainties of RES penetration, which in turn leads to diminished power quality concerns and instability [7]. There are two main classes of secondary control. The first is centralized, and the second is distributed. However, the distributed type can avoid such failures and be salable since it gathers information from local controllers [8]. A distributed secondary control mechanism tends to be applied

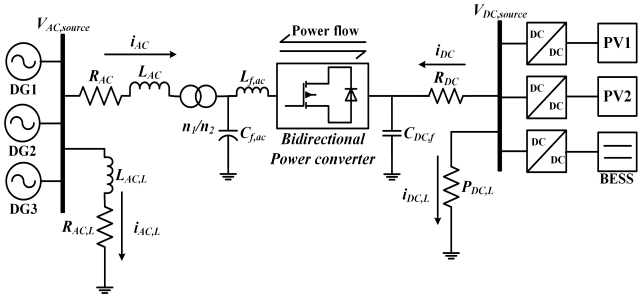

Fig. 1: Single line diagram of the shipboard microgrid

with the rapid development of microgrids and distribution generators (DGs). Similarly, a tertiary control's main purposes are to manage power flows and optimize the economic flow of energy by microgrids and utility grids when interconnected across the network [9].

The Sliding Mode Controller (SMC) controller is characterized as a robust controller. A variable structure control method could be used to ensure the Robustness of the entire system during transients due to the arbitrary transient impedances of voltage source converter (VSC). The autonomous Microgrid (MG) can be stabilized by controlling its motion and sable boundaries during fault ride-through. In this context, multi-agent power systems successfully testify to the sliding mode control [10].

Grid-Feeding Voltage Source Converters (GFD-VSC) need phase lock loop (PLL) synchronization units. The GFD-VSC must maintain a high level of stability and dynamic performance. An H_∞ robust control is employed in order to design a robust PLL with a dynamic state feedback controller. A feedback controller improves PLL stability and response when employed to control uncertainty and exogenous instabilities and disturbances [11]. An H_∞ robust controller is proposed as a replacement for the virtual impedance loop to suppress low-frequency oscillations and stabilize the autonomous networked microgrid. In [12], numerical and simulation results demonstrate the accuracy of the models.

The Interlinking Converter (IC) uses frequency-voltage droop control that incorporates the secondary AC control effect. Hence, ICs are critical components in SMG as they facilitate controlled and stable energy transmission and transformation between the AC and DC sides [13]. A robust control scheme for the hybrid AC/DC SMG is designed, implemented, and provided competitive analysis in this research to enhance multiple innovative hybrid AC/DC microgrid control configurations. On IC, a hierarchical primary and secondary controller is used to connect the AC Microgrid and DC microgrid to alleviate non-linearities during power fluctuations. IC secondary controller has proportional integral (PI) controllers and SMC. We will compare the performance of the secondary controller scheme [14].

This paper introduces a novel hierarchical control scheme for hybrid AC/DC shipboard microgrid systems, incorporating advanced control strategies to optimize the integration of RES such as solar and wind. The proposed system uniquely addresses the challenges posed by varying line impedances and unmeasured disturbances, particularly during dynamic load changes, by employing a robust secondary control architecture. The innovative aspect of this work lies in its dual-layer control mechanism that synergizes classical PI and SMC designs to maintain system stability and improve power quality under diverse grid conditions. This approach not only enhances the resilience and efficiency of shipboard microgrids but also contributes significantly to reducing carbon emissions by facilitating the seamless integration of RES into maritime power systems.

In this research study, the content of the research paper has been reorganized as follows. In section II, the problem formulation is done, where we discuss the modeling and design of the hybrid AC/DC SMG. In section III, the proposed hierarchical control scheme of the SMG system. Section VI provides the simulation results. Section V discusses the practical hardware implementation. Section VII gives a conclusion and future directions.

II. Modeling of Hybrid AC/DC Microgrid System

Microgrids are next-generation solutions of traditional power systems that facilitate two-way power flow and load management [15]. Electricity production, transmission, distribution, control centers, and consumers are the other components of the traditional power grid. In paper [16], two-way coordination services and the ability to use alternative energy sources more effectively are essential benefits of the microgrid system. Smaller areas may function independently or as an integral part of the grid with the help of microgrid systems [17]. Furthermore, enhanced service and control are offered to customers by microgrids equipped with sophisticated controls and tracking. In the grid-connected configuration, the microgrid is linked to the electrical network by a point of common coupling (PCC). The microgrid is able to function autonomously and fulfill control criteria autonomously [18]. When operating in isolated mode, microgrids provide a unique control challenge due to the need for multilayer management strategies to address technological limitations such as voltage, frequency, and protection limits.

On the basis of the power transmission type, there are three modes of microgrids that can be categorized as DC microgrid, AC microgrid, or hybrid AC/DC microgrid. The single line diagram (SLD) of a hybrid SMG structure is shown in Figure 1. The three distributed generators DG_1, DG_2, and DG_3 are thought to be linked to the AC bus $V_{AC,source}$, which supplies a AC local load $R_{AC,L}$ and $L_{AC,L}$. The associated DC load receives its source power from other DC panels and storage systems over the DC bus $V_{DC,source}$. To control the voltage, each DC source is linked to its own DC/DC converter. Between the AC and DC microgrid, there is an IC that connects them, and the transmission lines have a combined impedance of $R_{AC,line}$, $L_{AC,line}$, and $R_{DC,line}$. Although DC is only thought of as a constant resistive load, the AC load form may

be either static or dynamic. The IC makes it easier to control and transfer power in both directions [19].

The boost converter maintains a constant voltage even under extreme situations. What determines a three-phase LC filter are $L_{f,ac}$ and $C_{f,ac}$. Function $\omega_f = 1/\sqrt{L_{f,ac}\, C_{f,ac}}$ may be used to find the cutoff frequency of LC filters. The IC guarantees the two microgrids may transfer power in both directions, while the coupling capacitor $C_{f,dc}$ is used for rectification. According to the author [20], a DC source is considered to be functioning under optimal circumstances if it consistently provides a constant quantity of power or if it utilizes renewable energy resources at its maximum power point [21]. During a DC load, the quantity of power used is directly related to the amount of power that the consumer is consuming. When the DC power consumption goes above the dispatchable energy, it suggests that there is a chance [22]. Here, the AC power source is crucial for meeting the DC power requirement. The same holds true for the AC load. When it grows, the power consumption outstrips the AC supply, necessitating recovery of power from the DC source side to fulfill the demand [23].

A. AC Microgrid Modeling

To design a hybrid microgrid AC where AC loads R_L and L_L are connected. The electric current of type DGs powers the load. We may use Kirchhoff's Voltage Law (KVL) on the AC source side to get the equations. The research will demonstrate a hierarchical control structure for DG modules that consists of two levels [24]. The first level includes main controls that are based on droop, and the second level includes secondary controls that are used to restore voltage and frequency characteristics [25]. It is possible to get the source side equation from Figure 1 can be given as

$$V_{AC,source} = \{i_{AC} R_{AC} + V_{L_{AC}}\} + V_{AC,L} \tag{1}$$

where voltage across line impedance is the rate of change of line inductance.

$$V_{L_{AC}} = L_{AC} \frac{\mathrm{d}}{\mathrm{d}t} i_{AC} \tag{2}$$

so, (1) can be written as

$$V_{AC,source} = \{i_{AC} R_{AC} + L_{AC} \frac{\mathrm{d}}{\mathrm{d}t} i_{AC}\} + V_{AC,L} \tag{3}$$

By rearranging (3), we get

$$\frac{\mathrm{d}}{\mathrm{d}t} i_{AC} = \frac{1}{L_{AC}} (V_{AC,source} - V_{AC}) - \frac{R_{AC}}{L_{AC}} i_{AC} \tag{4}$$

Now, AC load side equation is the summation of voltages across load impedance.

$$V_{AC,L} = i_{AC,L}\ R_L + V_{L_L} \tag{5}$$

where

$$V_{L_L} = L_L\ \frac{\mathrm{d}}{\mathrm{d}t} i_{AC,L} \tag{6}$$

so, (5) can be written as

$$V_{AC,L} = i_{AC,L}\ R_L + L_L\ \frac{\mathrm{d}}{\mathrm{d}t} i_{AC,L} \tag{7}$$

By rearranging (7), we get

$$\frac{\mathrm{d}}{\mathrm{d}t} i_{AC,L} = \frac{V_{AC,L}}{L_L} - \frac{R_L}{L_L} i_{AC,L} \tag{8}$$

The $d-q$ state space model for (4) and (8) of AC network can be given as

$$\frac{\mathrm{d}}{\mathrm{d}t} i^d_{AC} = \frac{1}{L_{AC}} \left(V^d_{AC,source} - V^d_{AC,L}\right) + \omega i^q_{AC} - \frac{R_{AC}}{L_{AC}} i^d_{AC} \tag{9}$$

$$\frac{\mathrm{d}}{\mathrm{d}t} i^q_{AC} = \frac{1}{L_{AC}} \left(V^q_{AC,source} - V^q_{AC,L}\right) - \omega i^d_{AC} - \frac{R_{AC}}{L_{AC}} i^q_{AC} \tag{10}$$

$$\frac{\mathrm{d}}{\mathrm{d}t} i^d_{AC,L} = \frac{V^d_{AC,L}}{L_L} + \omega i^q_{AC,L} - \frac{R_L}{L_L} i^d_{AC,L} \tag{11}$$

$$\frac{\mathrm{d}}{\mathrm{d}t} i^q_{AC,L} = \frac{V^q_{AC,L}}{L_L} - \omega i^d_{AC,L} - \frac{R_L}{L_L} i^q_{AC,L} \tag{12}$$

B. DC Microgrid Modeling

On the DC microgrid, KVL is used to solve the DC load source side mathematical equations. Connecting a DC source to Battery Energy Storage Systems (BESS) that maintains a constant voltage is an example of a DC source. Moreover, a DC load never changes its power consumption [26]. The DC source voltage is equal to the total of the load voltage and the voltage along the losses in the transmission line, as stated by KVL at the DC MG.

$$V_{DC,source} = i_{DC} R_{DC} + V_{DC,L} \tag{13}$$

With a constant power demand, $P_{DC,L}$ stays the same, which is can be given as

$$V_{DC,source} = i_{DC} R_{DC} + \frac{P_{DC,L}}{i_{DC,L}} \tag{14}$$

Reducing the number of DG units needed is achieved by the use of RES to provide electric ship power. On the other hand, the efficiency of transmitting electricity to the consumption power system grows dramatically due to their inherent characteristics, most RES are equipped with BESS as the year progresses. A smooth and more dependable power-producing unit is achieved by using storage devices, such as batteries and fuel cells.

III. Proposed Robust Hierarchical Control Structure for Microgrid

The steady-state condition is directly affected by the short-term operation of primary and secondary controls. In order to get reliable steady-state analysis in AC/DC microgrid modeling, it is necessary to have both main and secondary controllers active. Hybrid SMG systems cannot operate without a reliable and appropriate method of power management, which allows for the regulation of load allocation among DC and AC power sources. Fewer attempts have been made in

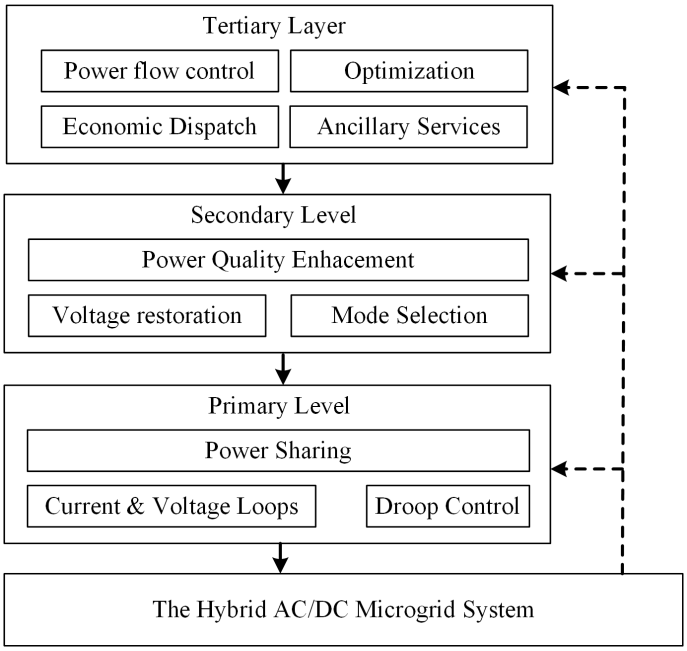

Fig. 2: Hierarchical control structure

power management between AC and DC power generations for hybrid systems till now while controlling power distribution in AC and DC microgrids. A reliable power-sharing method has been used to execute power-sharing control in microgrids. Multiple converters must work together to find the reference power that corresponds to the frequency droop characteristics [27]. All control modules are included in load balancing using the drooping slope technique. Figure 2 shows the flow of hybrid SMG hierarchical control design.

Centralized and decentralized controllers have been developed using a number of control algorithms, including H_∞, Linear Quadratic Regulator (LQR), sliding mode, model predictive control, and artificial intelligence techniques, including fuzzy logic, neural networks, and genetic programming.

Secondary control is the next logical step after this degree of control. The load variations in local voltage and global frequency are what secondary control is aiming to eradicate. There has been much research on centralized control systems in high-voltage transmission and distribution networks. Additional goals such as harmonic correction, reactive power-sharing, and voltage imbalance have been included in the secondary control [28]. The third level of control determines the worldwide economic dispatch across the network based on current energy prices and market circumstances.

The earlier works on control problem formulation considered only primary droop controls. However, higher control levels must be implemented in practical systems for the microgrid to function optimally and safely by using hierarchical control schemes. By including the comprehensive hierarchical control models, the solution obtained by applying the primary droop-controlled method in a controlled AC microgrid was determined to be the correct one in contrast to the solution

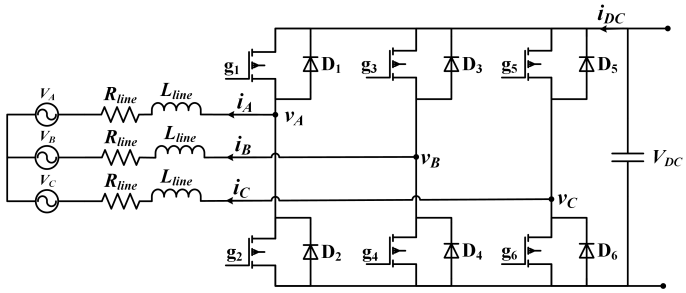

Fig. 3: Interlinking Voltage Source Converter (VSC) design

gained by using a hierarchical power flow model [29].

Technological advancements have facilitated the proliferation of microgrids in energy generation, control, computer hardware, and software utilization for microgrids. The advancement of MGs has been driven by industrial collaborations seeking to cut costs and boost their dependability and resiliency. Consequently, MGs is the dominant power source for many commercial and residential applications at present [30].

A. Modeling of Voltage Source Converter (VSC)

Figure 3 shows the three-phase VSC design for hybrid marine MG. The hierarchical control structure is managed by a two-level VSC device [31]. A voltage regulation controller is a key component of the main controller. Another option is to use the $(V - Q)$ to regulate the primary control layer. The inverter output voltage may be given using

$$V_{ABC} = v_{ABC} + R_{line} i_{ABC} + L_{line} \frac{\mathrm{d}}{\mathrm{d}t} i_{ABC} \tag{15}$$

So, the inverter output voltage is equal to the inverter instantaneous voltage plus the line inductance and resistance. We implemented a three-phase voltage system as an IC for a hybrid microgrid system. The three-phase root mean square (RMS) voltage is obtained straight from the AC bus or a three-phase transformer, without the need for any double-voltage capacitor [32]. In the aftermath of transits, the RMS voltage remains steady and stable throughout. Placing an LC filter network between the load and the AC bus becomes necessary. However, this study does not include filter design. As a result, we treated them as constants in statements.

$$\frac{\mathrm{d}}{\mathrm{d}t} i_{ABC} = \frac{V_{ABC}}{L_{line}} - \frac{R_{line}}{L_{line}} i_{ABC} - \frac{v_{ABC}}{L_{line}} \tag{16}$$

Applying dq-transformation of three phase currents.

$$\frac{\mathrm{d}}{\mathrm{d}t} i^d = \frac{V^d}{L_{line}} - \frac{v^d}{L_{line}} + \omega i^q - \frac{R_{line}}{L_{line}} i^d \tag{17}$$

and

$$\frac{\mathrm{d}}{\mathrm{d}t} i^q = \frac{V^q}{L_{line}} - \frac{v^q}{L} - \omega i^d - \frac{R_{line}}{L_{line}} i^q \tag{18}$$

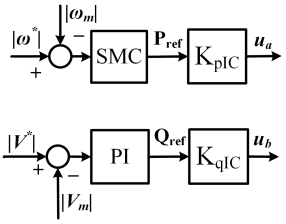

(a) SMC based secondary controller design

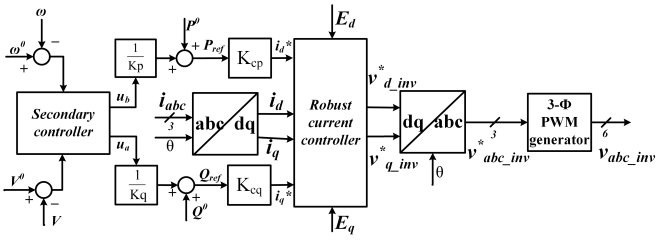

(b) Primary current controller design

Fig. 4: The current controller design

The state space model of (17) and (18) can be represent as

$$\begin{bmatrix}\dot{x}_1\\ \dot{x}_2\end{bmatrix} = \begin{bmatrix}-\frac{R_{line}}{L_{line}} & \omega\\ -\omega & -\frac{R_{line}}{L_{line}}\end{bmatrix}\cdot\begin{bmatrix}x_1\\ x_2\end{bmatrix} - \frac{1}{L_{line}}\begin{bmatrix}E^d\\ E^q\end{bmatrix} + \frac{1}{L_{line}}\begin{bmatrix}u_1\\ u_2\end{bmatrix} \tag{19}$$

B. Proposed Robust Controller Design and Analysis

The proposed robust architecture for the secondary controller is shown in Figure 4 (a). In this case, the primary controller design relied on a reliable SMC as a reference signal. With the primary controller's responsibility to reduce voltage and frequency droops, the secondary controller will provide its support to the primary controllers, as shown in Figure 4 (b), so that the power grids may contain even more robust synchronizations. In addition, the secondary controller guarantees that the load is constantly receiving the necessary amount of demand power. Under extreme changes in either the AC or DC loads, a standard control signal is provided by the secondary controller, which also keeps an eye on the voltage and frequency fluctuations in the hybrid grid. Hierarchical control structure u_ω and u_v are produced by processing the control signals P_{ref} and Q_{ref} with converter gains K_{pIC} and K_{qIC}, respectively.

Figure 4 (b) displays the traditional current controller system. The IC's voltage and frequency are controlled by the primary control design, which is based on droop control. The suggested robust secondary controller supplies the primary controller with reference signals u_ω and u_v in order to implement the hierarchical control design. The droop controller will generate $v_{abc,inv}$ gating pulses by monitoring the grid voltage and frequency. The voltages are E^d_{inv} and E^q_{inv}. A three-phase v_{inv} inverter signal for the Pulse Width Modulation (PWM) generator is generated by processing the park inverse transformation by use of v_d inverter signals that are produced by the robust current controller. The suggested rule for secondary control may be expressed as

$$u_v = -\beta(x)\ sat\left(\frac{s}{\mu}\right) \tag{20}$$

If $\mu = 0.05$, then the control signal is u_v, the controller gain is β, and the sliding surface is s. Therefore, the applicable control regulations in this instance might be depicted as

$$i_q = -Ksat(s/\mu) \tag{21}$$

and

$$u_\omega = K_p + \int K_i \cdot \mathrm{d}t\ (\omega^*_{inv} - \omega_{inv}) \tag{22}$$

errors between output and reference can be given as

$$e^d = i^{d*}_{AC,L} - i^d_{AC,L} \tag{23}$$

$$e^q = i^{q*}_{AC,L} - i^q_{AC,L} \tag{24}$$

At the AC load equations can be given as, $i^d_{AC,L}$ and $i^q_{AC,L}$ are located. The reference currents are $i^{d*}_{AC,L}$ and $i^{q*}_{AC,L}$. There will be a sliding surface s.

$$s = K_0 \int e^q \cdot \mathrm{d}t + e^q \tag{25}$$

$$s = K_0 \int (i^{q*}_{AC,L} - i^q_{AC,L}) \cdot \mathrm{d}t + (i^{q*}_{AC,L} - i^q_{AC,L}) \tag{26}$$

Sliding surface s derivative is

$$\dot{s} = K_0(i^{q*}_{AC,L} - i^q_{AC,L}) + \left(\frac{\mathrm{d}}{\mathrm{d}t}i^{q*}_{AC,L} - \frac{\mathrm{d}}{\mathrm{d}t}i^q_{AC,L}\right) \tag{27}$$

at constant reference value,

$$i^{q*}_{AC,L} = \frac{\mathrm{d}}{\mathrm{d}t}i^q_{AC,L} = 0 \tag{28}$$

referring (27)

$$\dot{s} = -K_0 i^q_{ABC} - \frac{\mathrm{d}}{\mathrm{d}t}i^q_{ABC} \tag{29}$$

From (18)

$$\dot{s} = -K_0 i^q + \frac{V^q}{L_{line}} - \frac{V^q}{L_{line}} + \frac{R_{line}}{L_{line}}i^q + \omega_{inv} i^d \tag{30}$$

Rearranging the terms,

$$\dot{s} = \frac{V^q}{L_{inv}} - \frac{V^q}{L_{line}} + \omega i^d + \left(\frac{R_{line}}{L_{line}} - K_0\right)i^q \tag{31}$$

simplified form can be given as

$$\dot{s} = \chi_{line} + \psi i^q \tag{32}$$

where

$$\chi = \left(\frac{V^q}{L_{inv}} - \frac{V^q}{L_{line}} + \omega_{inv} i^d\right) \tag{33}$$

$$\psi = \left(\frac{R_{line}}{L_{line}} - K_0\right) \tag{34}$$

The condition for ψ to satisfy is

$$\psi \geqslant \psi_0 \geqslant 0 \tag{35}$$

Here ψ_0 is a constant that is positive. Next, we will choose a suitable Lyapunov function $V(x) \in \mathbb{R}^1$ for the stability assessment of our designed control

$$V(x) = \frac{1}{2}s^2 \tag{36}$$

Then

$$\dot{V}(x) = s\dot{s} \tag{37}$$

From (32)

$$\dot{V}(x) = s\chi + s\psi i^q \tag{38}$$

Chattering can be reduced by choosing s as,

$$\mid s \mid \geqslant \mu \tag{39}$$

Where μ is a very small positive value. The closed-loop control law equation will be

$$i_q = -Ksgn(s) \tag{40}$$

Substituting (40) into (38), we get

$$\dot{V}(x) = s\chi - sK\psi sgn(s) \tag{41}$$

$$\dot{V}(x) = \psi\frac{s\chi}{\psi} - sK\psi \mid s \mid \tag{42}$$

or

$$\dot{V}(x) \leqslant \psi \mid s \mid \left|\frac{\chi}{\psi}\right| - K\psi \mid s \mid \tag{43}$$

where

$$\left|\frac{\chi}{\psi}\right| \leqslant K - K_0 \tag{44}$$

Since K_0 is a positive constant, we have

$$\forall \quad K \geqslant K_0 + \left|\frac{\chi}{\psi}\right| \tag{45}$$

Now, by substituting values of in (44) into (43), we get

$$\dot{V}(x) \leqslant -K_0\xi_0 \mid s \mid \tag{46}$$

Equation (46) guarantees that the suggested controller will be a strong stabilizing controller satisfying the requirements in (44). Computational gains used in the controller are shown in Table I.

TABLE I: Controller design

Parameters	Description	Values
K_P	Proportional gain	0.1
K_I	integral gain	5
K_0	SMC gain	0.8
β	Sliding surface gain in SMC	0.05
μ	Sliding manifold boundary	0.6

IV. Simulation Results

We used the Matlab/Simulink tool for the microgrid implementation and testing of our proposed controller. For the simulation platform, we developed the AC and DC power generation units and loads of microgrid systems. On the AC MG side, we used three identical DGs with having 16 $kVar$ power rating and 400 volts three-phase RMS voltage. The DGs are connected to a bus with its local AC loads. Three distinct 5 kW active loads with 3 $kVar$ inductive load in parallel are used with the circuit breaker combining the transmission line lumped impedances. The AC microgrid follows the 50 Hz operating frequency. In addition, power can be sent to either side of the grid as needed by the load due to the IC, which is a 2-level VSC. PV and BESS are examples of DC sources, whereas DC resistive loads and transmission lines with resistance make up a DC microgrid. The DC bus voltage is 450 volts. Three identical resistive loads are connected to it through a circuit breaker. DC load we using is 250 W each. The hierarchical controller uses AC and DC line current feedback to produce commands for the primary controller, which renders the IC. Simulation parameters are given in Table II.

TABLE II: Hybrid microgrid system parameters

Parameters	Description	Values
$v_{DC,source}$	DC source side voltage	500 volts
$v_{AC,source}$	AC source side voltages	400 volts
f_{grid}	AC grid frequency	50 Hz
$P_{DC,L}$	power of DC load	250 W
$P_{AC,L}$	Active power load	6 kW
$Q_{AC,L}$	Reactive power load	3 kVar
f_{inv}	VSC frequency	8 kHz

A. Case 1: Power flow from AC to DC; then DC to AC side

The power flow analysis of the hybrid SMG has been simulated using MATLAB/Simulink to compare the performance of conventional PI and proposed robust secondary control schemes. At simulation time $t = 0.5$ sec, we took into account the transition from the AC grid to the DC grid.

The variations of AC active load power in the hybrid SMG are shown in Figure 5 (a). The blue line represents the secondary controller reaction based on PI, whereas the orange line represents the response based on SMC. Initially, the IC will function as a rectifier and meet the AC and DC load power requirements while the grid is run by an AC microgrid. Utilizing a conventional PI controller regulates the load power to 4.2 kW for a duration $0 \leqslant t < 0.5$ sec, while the proposed SMC based secondary control achieves a better response, regulated to 4.8 kW. $\Delta P_{droop} = 600W$ is the result of comparing the load power. After that, because the AC sources are disconnected, the power is supplied to the DC and AC loads by the PV between 0.5 $sec < t \leqslant 1$ sec. Here, we can analytically observe that during this inverter mode, the PI based controller has AC load power deviation

that remains same compared to SMC based controller. Furthermore, we can notice a significant voltage drop improvement by employing a secondary controller strategy. Maximum voltage droop using PI controller is $P_{AC,L}^{PI} = 3.2\ kW$ greater than SMC based controller which is $P_{AC,L}^{SMC} = 2.7\ kW$. Hence, $\Delta P_{droop} = 1.1\ kW$.

Figure 5 (b) shows the reactive power waveform. Here we can see that from $0\ sec < t \leqslant 0.5\ sec$, the reactive power is $2.4\ kVar$ and $2.3\ kVar$ with SMC and PI based controller respectively. After the grid transition, the reactive power becomes $2.3\ kVar$ and $2.2\ kVar$ with SMC and PI based controller, respectively. The reactive power droop due to grid transition in case of SMC is $Q_{AC,L}^{SMC} = 1\ kVar$ and with PI $Q_{AC,L}^{SMC} = 1.7\ kVar$. Hence, $\Delta Q_{droop} = 800\ Var$.

In Figure 5 (c), the frequency changes on the AC grid are shown. As opposed to traditional control, the results of controlling the frequency and steady-state performance from controllers based on SMC are superior. The SMC based controller is smoothly controlled at $50\ Hz$, in contrast to the PI-based controller, which exhibits frequency changes $\Delta f_{droop}^{1} = 0.09\ Hz$ and $\Delta f_{droop}^{2} = 0.05\ Hz$ which shows better performance of our proposed control scheme.

Figure 5 (d) shows DC load waveform which is regulated at $P_{DC,L} = 250\ W$. Here, DC load is getting power from AC source from $0\ sec < t \leqslant 0.5\ sec$. After that, it gets power from DC source, which is stable and same. We also observed harmonics due to inverter switching in IC.

B. Case 2 : Power flow from DC to AC ; then AC to DC side

The fluctuation in active load power caused by microgrid changeover is shown in Figure 6 (a) compared to the traditional method and the robust secondary controller. The AC load power is initially limited to $5.5\ kW$ since the grid is functioning from a DC source. Then at $t = 0.3\ sec$, step load decreases to $3.9\ kW$, and at $t = 0.7\ sec$, the step load further decrement to $2.2\ kW$. A power droop due to voltage droops is seen after time $t = 0.5\ sec$ when grid changeover occurs. Using the traditional secondary controller method resulted in an active power droop of $P_{AC,L}^{PI} = 3.4\ kW$. Nevertheless, the power decrease of $P_{AC,L}^{SMC} = 1.1\ kW$ caused by the grid changeover is an improvement by SMC $\Delta P_{droop} = 2.3\ kW$.

Figure 6 (b) shows the reactive power waveform. Here we can see that the reactive power droop due to grid transition in case of SMC is $Q_{AC,L}^{SMC} = 900\ Var$ and with PI $Q_{AC,L}^{SMC} = 500\ kVar$. Hence, we observe $\Delta Q_{droop} = 500\ Var$.

The frequency differences caused by microgrid switching are compared in Figure 6 (c) between the traditional method and the proposed secondary controller-based method. At the beginning, the grid is running on a DC supply. Therefore after time $t = 0.5$ seconds, it aims to stabilize and control its frequency at $50\ Hz$. We see frequency drops in both kinds of secondary controllers that are $\Delta f_{droop}^{1} = 0.1\ Hz$ and $\Delta f_{droop}^{2} = 0.03\ Hz$, showing better performance of our proposed control scheme. We observed that the SMC based secondary controller approach leads to far better frequency droop steady-state responsiveness.

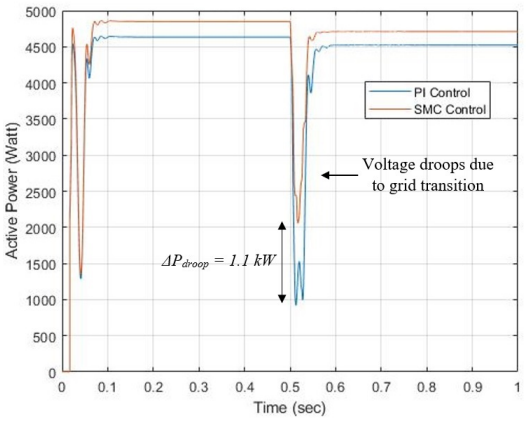

(a) Active power Variations at AC load

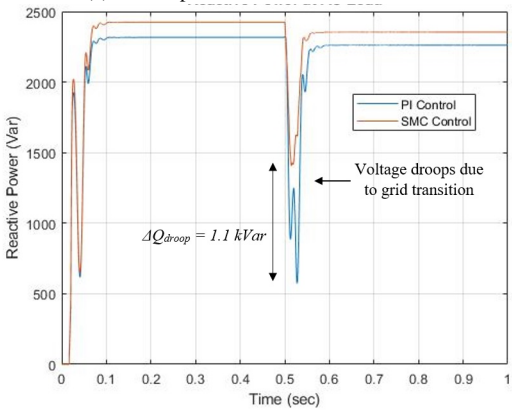

(b) Reactive power variations at AC load

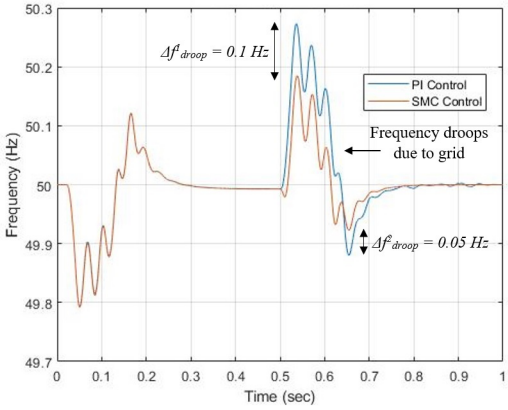

(c) Frequency variations at AC load

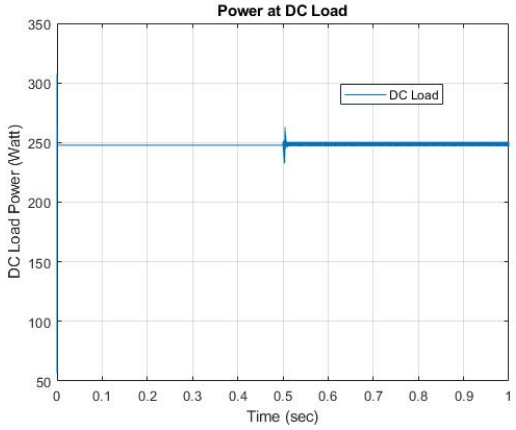

(d) DC load power variations

Fig. 5: Case 1 : Power flow from AC to DC side then DC to AC side comparisons

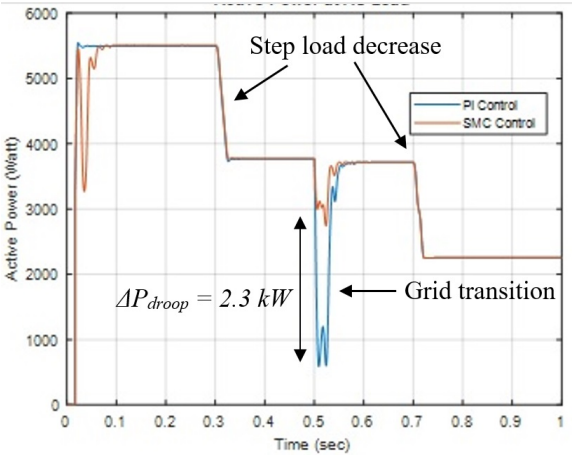

(a) Active power variations at AC load

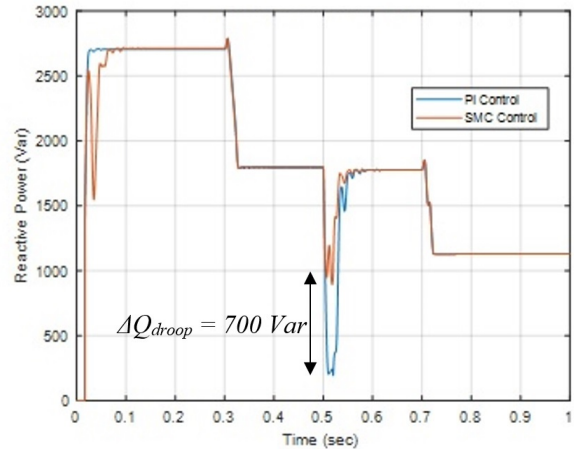

(b) Reactive power variations at AC load

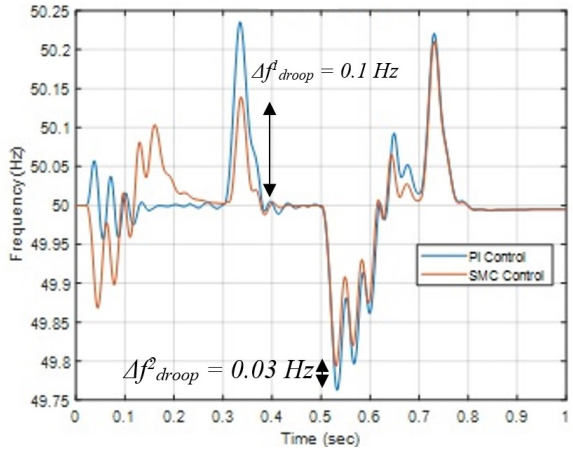

(c) Frequency variations at AC load

Fig. 6: Case 2 : Power flow from DC to AC side then AC to DC side load variations comparisons

V. Hardware Implementations

A. Hardware Setup

In the experimental setup of the hybrid AC/DC microgrid Supervisory SMC-based controller for the interlinking converter, the Jetson Nano board serves as a powerful and versatile computing platform. Its compact size, low power consumption, and high computational capabilities make it an ideal choice for real-time control applications in microgrid systems. The Jetson Nano is equipped with a quad-core ARM Cortex-A57 CPU and an NVIDIA Maxwell GPU with 128 CUDA cores [33]. These components provide sufficient computational power to execute Hardware-in-the-loop (HIL), complex control algorithms, and optimization routines required for supervisory control in the hybrid shipboard microgrid [34].

The control algorithms, including the hierarchical control design and the supervisory model predictive controller, are implemented on the Jetson Nano using programming languages such as Python or C/C++. The Jetson Nano's compatibility with popular development frameworks like TensorFlow and PyTorch enables seamless integration of advanced control algorithms, machine learning models, and optimization techniques. The Jetson Nano facilitates communication with other components of the microgrid, such as power converters, energy storage systems, and external control systems [35]. It supports various communication protocols like Ethernet, CAN bus, and serial communication, enabling seamless integration and coordination of disparate components within the microgrid. Specifically, the Jetson Nano orchestrates the power exchange between AC and DC subsystems of the microgrid intelligently controlled through the bidirectional IC through HIL. It regulates the converter's operation based on the supervisory control decisions, ensuring efficient power sharing and management while maintaining system stability and reliability. Figure 7a shows the block diagram of hardware implementation.

The Jetson Nano's modular architecture allows for scalability and flexibility in the design and implementation of the microgrid control system. Additional computational resources can be added as needed to accommodate future expansions or upgrades to the microgrid infrastructure. Figure 7b shows the hardware setup we developed to test the performance of controllers for the hybrid AC/DC microgrid system.

B. Hardware Results

Hardware results comparison of PI and SMC based control schemes for microgrid are shown in Figure 8 and Figure 9. In Figure 8 (a), we consider the gird transition case 1 in which power is initially flowing from AC to DC side then at $t = 0.5\ sec$, DC to AC side. Here, we observed that the $\Delta P_{droop} = 1\ kW$.

The frequency variations caused by microgrid switching are compared in Figure 8 (b) between the traditional method and the proposed secondary controller-based method.

Figure 8 (c) shows DC load waveform which is regulated at $P_{DC,L} = 250\ W$. Here, DC load is getting power from AC source from $0\ sec < t \leqslant 0.5\ sec$. After that, it gets

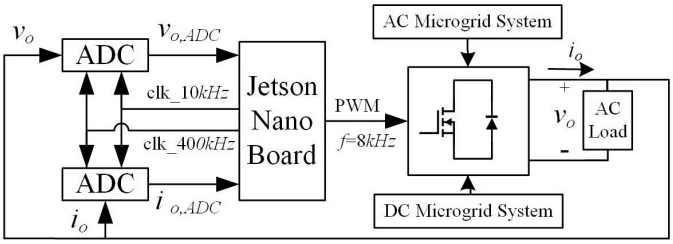

(a) Hardware block diagram design

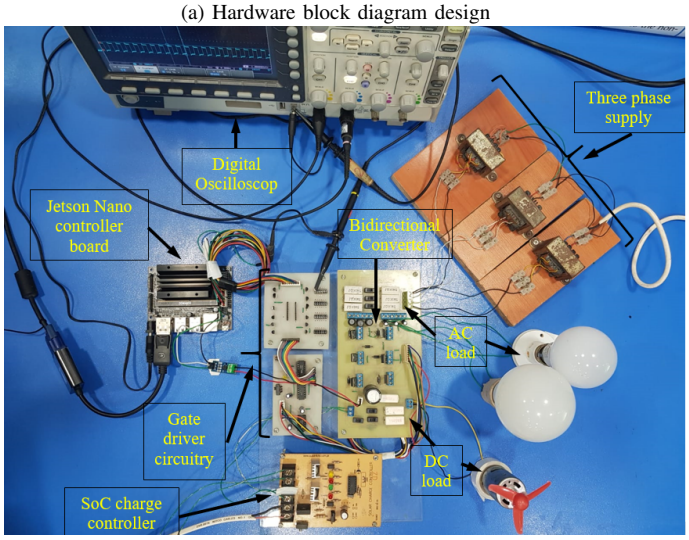

(b) Hardware setup

Fig. 7: Hardware implementations

power from DC source, which is stable and the same. We also observed harmonics due to inverter switching in IC.

Similarly, in Figure 9 (a), we consider the gird transition case 2 in which power is initially flowing from DC to AC side, then at $t = 0.5\ sec$, AC to DC side with identical load increments at $t = 0.3\ sec$ and $t = 0.7\ sec$. Here, we observed that the $\Delta P_{droop} = 1\ kW$.

The frequency variations caused by microgrid switching are compared in Figure 9 (b) between the traditional method and the proposed secondary controller-based method.

Figure 9 (c) shows DC load waveform which is regulated at $P_{DC,L} = 250\ W$. Identical step DC load increased at $t = 0.3\ sec$ and $t = 0.7\ sec$. After that, it gets power from AC source, which is stable and the same. We also observed harmonics due to inverter switching in IC.

VI. Conclusion

With increased electrical power demand associated with carbon emissions, renewable energy integration with shipboard microgrids provides a better solution. In this research, we proposed an intelligent hierarchical control of the voltage and frequency droops in the bidirectional interlinking converter for the shipboard microgrid applications. The point is to reduce carbon emissions and produce an efficient power supply. Hence, our proposed method is robust to dynamical load variations for the hybrid AC/DC microgrid. The hybrid microgrid system described in this work uses a robust hier-

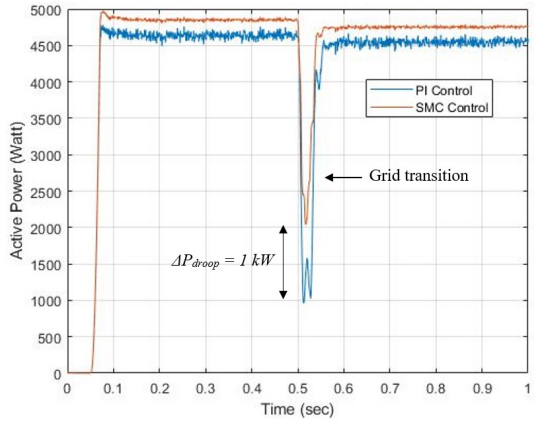

(a) Active power variations at AC load

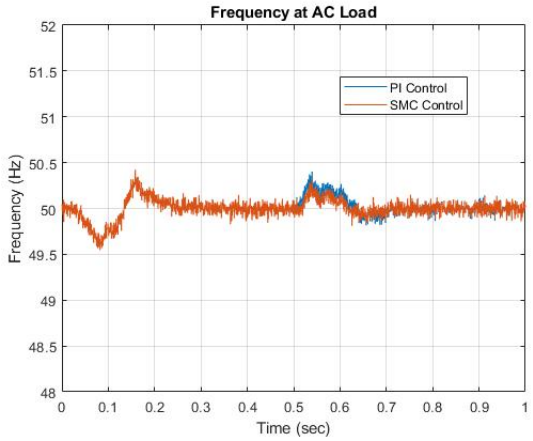

(b) Frequency variations at AC load

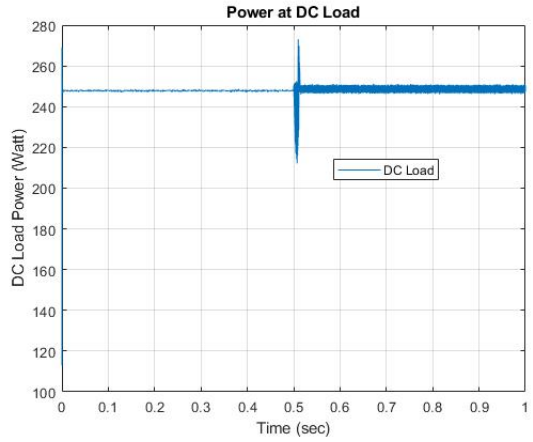

(c) DC load voltage variations

Fig. 8: Case 1 : Practical results of power flow from AC to DC side then DC to AC side comparisons

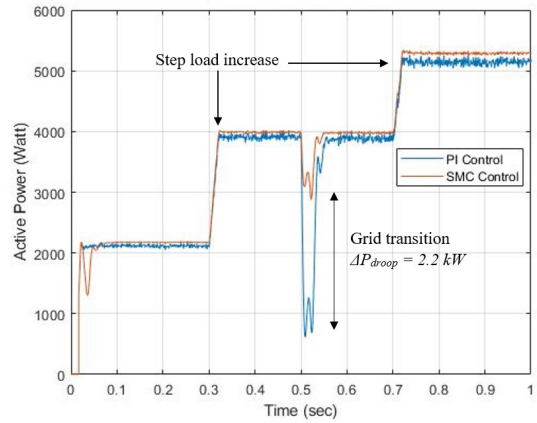

(a) Active power variations at AC load

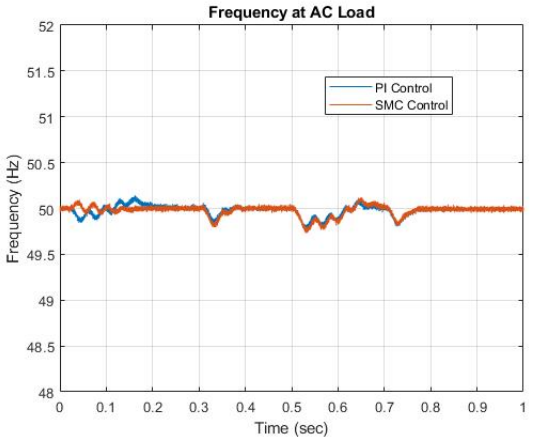

(b) Reactive power variations at AC load

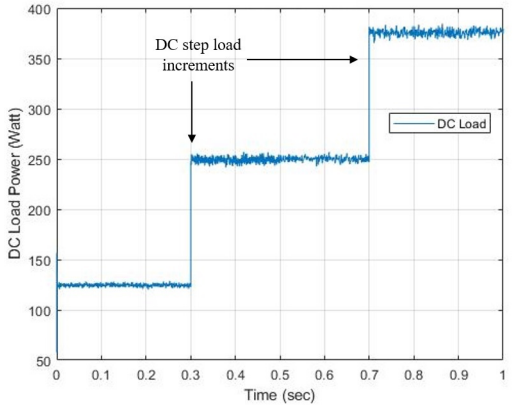

(c) Frequency variations at AC load

Fig. 9: Case 2 : Practical results of power flow from DC to AC side then AC to DC side comparisons

archical controller to integrate several microgrids with RES for power management and quality enhancement. The novelty of this work lies in its secondary layer control mechanism that synergizes classical PI and SMC designs to maintain system stability and improve power quality under diverse grid conditions. Our research is further distinguished by its comprehensive validation through both simulation in MATLAB/SIMULINK and practical implementation on hardware setups, demonstrating the feasibility and effectiveness of the control schemes in real-world scenarios. Developing an IC with a suitable control technique that can enable the SAF to decrease harmonics and offer reactive power correction with appropriate energy control is one of the obstacles encountered throughout the process.

REFERENCES

[1] Kiran, N. (2014). Sliding Mode Control of Buck Converter. Buletin Teknik Elektro dan Informatika(Bulletin of Electrical Engineering and Informatics), 37-44..

[2] Saoudi, M., El-Sayed, A., Metwally, H. (2017). Design and Implementation of Closed-Loop Control System for Buck converter Using different techniques. IEEE A and E SYSTEMS MAGAZINE, 30-39.

[3] Das, A.,Namboothiripad, M. K. (2014). Voltage Control of Buck Converter using Sliding Mode Controller. International Journal of Engineering Research Technology (IJERT), 1619-1623.

[4] Hashmi, S. M., Memon, A. Y. (2020). Simulation of PWM based Sliding Mode Controller for a DC-DC Buck Converter on FIL. IEEE Xplore, 344-349.

[5] A. Rehmat, F. Alam, M. Nasir and S. S. Zaidi, "Robust Hierarchical Non-linear Droop Control Design for the PV based Islanded Microgrid," 2022 19th International Bhurban Conference on Applied Sciences and Technology (IBCAST), Islamabad, Pakistan, 2022, pp. 620-628, doi: 10.1109/IBCAST54850.2022.9990397.

[6] Yamashita, Daniela Yassuda, Ionel Vechiu, and Jean-Paul Gaubert. "A review of hierarchical control for building microgrids." Renewable and Sustainable Energy Reviews 118 (2020): 109523.

[7] Ali, Waleed, et al. "Hierarchical control of microgrid using IoT and machine learning based islanding detection." IEEE Access 9 (2021): 103019-103031.

[8] Khan, Shahzad, et al. "Artificial intelligence framework for smart city microgrids: State of the art, challenges, and opportunities." 2018 third international conference on Fog and Mobile Edge Computing (FMEC). IEEE, 2018.

[9] Chui, Kwok Tai, Miltiadis D. Lytras, and Anna Visvizi. "Energy sustainability in smart cities: Artificial intelligence, smart monitoring, and optimization of energy consumption." Energies 11.11 (2018): 2869.

[10] Nair, Divya R., Manjula G. Nair, and Tripta Thakur. "A smart microgrid system with artificial intelligence for power-sharing and power quality improvement." Energies 15.15 (2022): 5409.

[11] Sabzehgar, Reza, Diba Zia Amirhosseini, and Mohammad Rasouli. "Solar power forecast for a residential smart microgrid based on numerical weather predictions using artificial intelligence methods." Journal of Building Engineering 32 (2020): 101629.

[12] Hasija, Sameer, and Chung Piaw Teo. "Introduction to the Special Section on Smart City Operations." Manufacturing & Service Operations Management 24.5 (2022): 2387-2388.

[13] Mohammadi, Ebrahim, et al. "A review on application of artificial intelligence techniques in microgrids." IEEE Journal of Emerging and Selected Topics in Industrial Electronics (2022).

[14] Jayashree, S., and K. Malarvizhi. "AI-Based Smart Micro Grids." Advanced Controllers for Smart Cities. Springer, Cham, 2021. 1-14.

[15] Kundu, Debasish. "Blockchain and trust in a smart city." Environment and Urbanization ASIA 10.1 (2019): 31-43.

[16] Albarakati, Aiman J., et al. "Real-time energy management for DC microgrids using artificial intelligence." Energies 14.17 (2021): 5307.

[17] Omitaomu, Olufemi A., and Haoran Niu. "Artificial intelligence techniques in smart grid: A survey." Smart Cities 4.2 (2021): 548-568.

[18] Omitaomu, Olufemi A., and Haoran Niu. "Artificial intelligence techniques in smart grid: A survey." Smart Cities 4.2 (2021): 548-568.

[19] Kanase-Patil, Amarsingh B., et al. "A review of artificial intelligence-based optimization techniques for the sizing of integrated renewable energy systems in smart cities." Environmental technology reviews 9.1 (2020): 111-136.
[20] Herath, Pramod Uthpala, et al. "Computational intelligence-based demand response management in a microgrid." IEEE Transactions on Industry Applications 55.1 (2018): 732-740.
[21] Song, Yonghua, et al. "Resilient power grid for smart city." iEnergy 1.3 (2022): 325-340.
[22] Nammouchi, A., Aupke, P., Kassler, A., Theocharis, A., Raffa, V., & Di Felice, M. (2021, September). Integration of AI, IoT and edge-computing for smart microgrid energy management. In 2021 IEEE International Conference on Environment and Electrical Engineering and 2021 IEEE Industrial and Commercial Power Systems Europe (EEEIC/I&CPS Europe) (pp. 1-6). IEEE.
[23] Marín Quintero, J. G. (2022). Adaptive protection in active distribution networks using local information.
[24] Sarangi, R. R., Pradhan, A., Moharana, J., Ray, P. K., & Mohanty, A. (2023, December). Rate of Change of Frequency Detection in Microgrid under Stochastic Supply and Load. In 2023 IEEE 3rd International Conference on Smart Technologies for Power, Energy and Control (STPEC) (pp. 1-5). IEEE.
[25] Marin-Quintero, J., Orozco-Henao, C., Bretas, A. S., Velez, J. C., Herrada, A., Barranco-Carlos, A., & Percybrooks, W. S. (2022). Adaptive fault detection based on neural networks and multiple sampling points for distribution networks and microgrids. Journal of Modern Power Systems and Clean Energy, 10(6), 1648-1657.
[26] Rodriguez, D. F., Alvarez, D. L., Gomez, D., Gers, J. M., & Rivera, S. (2021, February). Low-cost analysis of load flow computing using embedded computer empowered by gpu. In 2021 IEEE Power & Energy Society Innovative Smart Grid Technologies Conference (ISGT) (pp. 1-5). IEEE.
[27] Gozuoglu, A., Ozgonenel, O., & Gezegin, C. (2024). CNN-LSTM Based Deep Learning Application on Jetson Nano: Estimating Electrical Energy Consumption for Future Smart Homes. Internet of Things, 101148.
[28] Trivedi, R., & Khadem, S. (2022). Implementation of artificial intelligence techniques in microgrid control environment: Current progress and future scopes. Energy and AI, 8, 100147.
[29] Wu, T., & Wang, J. (2021). Artificial intelligence for operation and control: The case of microgrids. The Electricity Journal, 34(1), 106890.
[30] Wu, T., & Wang, J. (2021). Artificial intelligence for operation and control: The case of microgrids. The Electricity Journal, 34(1), 106890.
[31] Akpolat, A. N., Habibi, M. R., Dursun, E., Kuzucuoğlu, A. E., Yang, Y., Dragičević, T.,& Blaabjerg, F. (2020). Sensorless control of DC microgrid based on artificial intelligence. IEEE Transactions on Energy Conversion, 36(3), 2319-2329.
[32] Nair, D. R., Nair, M. G., & Thakur, T. (2022). A smart microgrid system with artificial intelligence for power-sharing and power quality improvement. Energies, 15(15), 5409.
[33] Manolescu, D., Reid, D., & Secco, E. L. (2024, March). Hardware and Software Integration of Machine Learning Vision System Based on NVIDIA Jetson Nano. In Future of Information and Communication Conference (pp. 129-137). Cham: Springer Nature Switzerland.
[34] Carbone, A., Spiller, D., Farissi, M. S., Sasidharan, S. T., Latorre, F., & Curti, F. (2022, September). Hardware-in-the-Loop Simulations of Future Autonomous Space Systems Aided by Artificial Intelligence. In International Conference on Applied Intelligence and Informatics (pp. 83-99). Cham: Springer Nature Switzerland.
[35] Pont-Esteban, D., Contreras-González, A. F., Samper-Escudero, J. L., Sáez-Sáez, F. J., Ferre, M., & á Sánchez-Urán, M. (2021, February). Validation of an elbow position super-twisting sliding-mode controller for upper-limb exosuit using a soft position sensor. In Journal of Physics: Conference Series (Vol. 1828, No. 1, p. 012074). IOP Publishing.